Modeling of All-Solid-State thin-film Li-ion Batteries:

accuracy improvement

Namdar Kazemi[a], Dmitri L. Danilov[b,c,*], Lucas Haverkate[a], Nancy J. Dudney[d],

Sandeep Unnikrishnan[a] and Peter H. L. Notten[b,c,e]

[a] *Holst Centre/Imec, High Tech Campus 31, 5656 AE Eindhoven, The Netherlands*

[b] *Eindhoven University of Technology, P.O. Box 513, 5600 MB Eindhoven, The Netherlands*

[c] *Forschungszentrum Jülich (IEK-9), Ostring O10, 52425 Jülich, Germany*

[d] *Oak Ridge National Laboratory, P.O. Box 2008, Oak Ridge, TN 37831-6124*

[e] *University of Technology Sydney, Broadway, Sydney, NSW 2007, Australia*

* Corresponding author:

Dr. Dmitri L. Danilov

Forschungszentrum Jülich (IEK-9),

Ostring O10, 52425 Jülich, Germany

Email address: d.danilov@fz-juelich.de

Declaration of interest: none

1

Abstract

Thin-film Solid-State Batteries (TFSSB) is one of most promising and quickly developing fields in modern electrochemical energy storage. Modeling these devices is interesting from theoretical and practical point of view. This paper represents a simulation approach for TFSSB which overcome a major drawback of available mathematical models, *i.e.* decline in accuracy of the models at high current rates. A one-dimensional electrochemical model, including charge transfer kinetics on the electrolyte-electrode interface, diffusion and migration in electrolyte as well as diffusion in intercalation electrode has been developed and the simulation results are compared to experimental voltage-capacity measurements. A new definition of diffusion coefficient as a function of concentration, based on the experimental measurements, is used to improve the performance of the model. The simulation results fit the available experimental data at low and high discharge currents up to 5 mAh cm^{-2}. The models show that the cathode diffusion constant is a prime factor limiting the rate capability for TFSSB in particular for ultrafast charging applications.

Introduction

Due to the high energy and power density of lithium-ion batteries they have become the technology of choice for consumer electronics, medical application, space applications and hybrid electrical vehicles (HEV). They are a promising candidate for sustainable and green technology. Nowadays electrochemical power sources made significant improvements in design, economy, energy density and operation life [1, 2]. Since their introduction in 1991, lithium-ion batteries with liquid electrolyte are vastly commercialized [3]. The global market for lithium-ion batteries at $9.4 billion in 2011 is expected to reach $18.6 billion by 2017 [4]. Major challenges in performance and safety of liquid-based and gel-type lithium-ion batteries, including the thermal stability of active materials within the battery at high temperatures, and the occurrence of internal short circuits that may lead to thermal runaway (see [5]) has drawn the attention to solid-state lithium-ion batteries [6]. Solid state batteries still work in the same way as current batteries do, but the change in materials alters some of the battery's attributes, including maximum storage capacity, charging times, size, and safety. Modeling solid-state batteries draw considerable attention of researchers. Danilov, *et al.* [7] developed an isothermal model for thin-film solid-state batteries (TFSSB), which includes diffusion and migration of ions in the electrolyte, the charge-transfer kinetics at the

electrolyte/electrode interface and Li-ion diffusion in the intercalation cathode. A number of other modeling approaches followed [8-11].

Among the physical properties of the lithium-ion batteries, the diffusion coefficient is the most important and interesting property in a conventional lithium-ion battery. The diffusion coefficient describes how easy ions can move in the electrolyte and electrode lattice. Since the limiting factor in the performance of lithium-ion batteries is reaching the maximum concentration of lithium on the electrolyte-electrode interface, choosing the right value for the diffusion coefficient is of great importance. Experimental and mathematical methods have been used to study the diffusion coefficient of lithium in common cathodes, reported values vary between 10^{-7} to 10^{-13} cm^2 s^{-1} [12-17]. The broad range of reported values are, in addition to different material properties, due to the different measurement techniques and different assumptions for geometrical factors used in the calculations. Van der Ven, *et al.* [18] used first principles electronic structure methods and Monte-Carlo simulations to investigate the atomistic mechanisms of lithium diffusion, the simulations resulted in a minimum diffusion coefficient for composition $Li_{0.5}CoO_2$. Jang, *et al.* [13] measured the diffusion coefficient for two batteries with $LiCoO_2$ cathodes, using potentiostatic intermittent titration technique (PITT). Dokko, *et al*. [12] performed impedance measurements on single particle LiCoO$_2$ electrodes and reported the diffusion as well as other ionic and electronic transport properties. Tang, *et al.* [19] used electrochemical impedance spectroscopy (EIS) and PITT to measure the diffusion coefficient in a (003) oriented LiCoO$_2$ thin film cathode prepared by pulsed laser deposition (PLD). Bouwman, *et al.* [20] studied the effect of plane orientation on the lithium intercalation in cathode and measured the diffusion coefficient for RF sputtered thin film cathodes exhibiting an a-axis orientation with favorable lithium diffusion channel perpendicular to the substrate and PLD thin film cathodes with a plane orientation parallel to the substrate.

In the present study, the same charge transport mechanisms are used as in [7], but a new concentration dependent diffusion coefficient is taken into account to make the model more accurate compared to older models simulating batteries. The results are compared with the experimental data reported in the open literatures and other numerical solutions.

Theoretical description

Fig. 1 schematically depicts a solid state lithium-ion battery. This cell consists of metallic lithium foil (Li) and lithium cobalt oxide ($LiCoO_2$ or LTO) as anode and cathode, respectively, which are

separated by a solid state lithium phosphate (Li_3PO_4 or LIPO) as electrolyte. The chemical reactions occurring at the surfaces of the positive and negative electrodes are given by Eqs. 1 and 2 respectively:
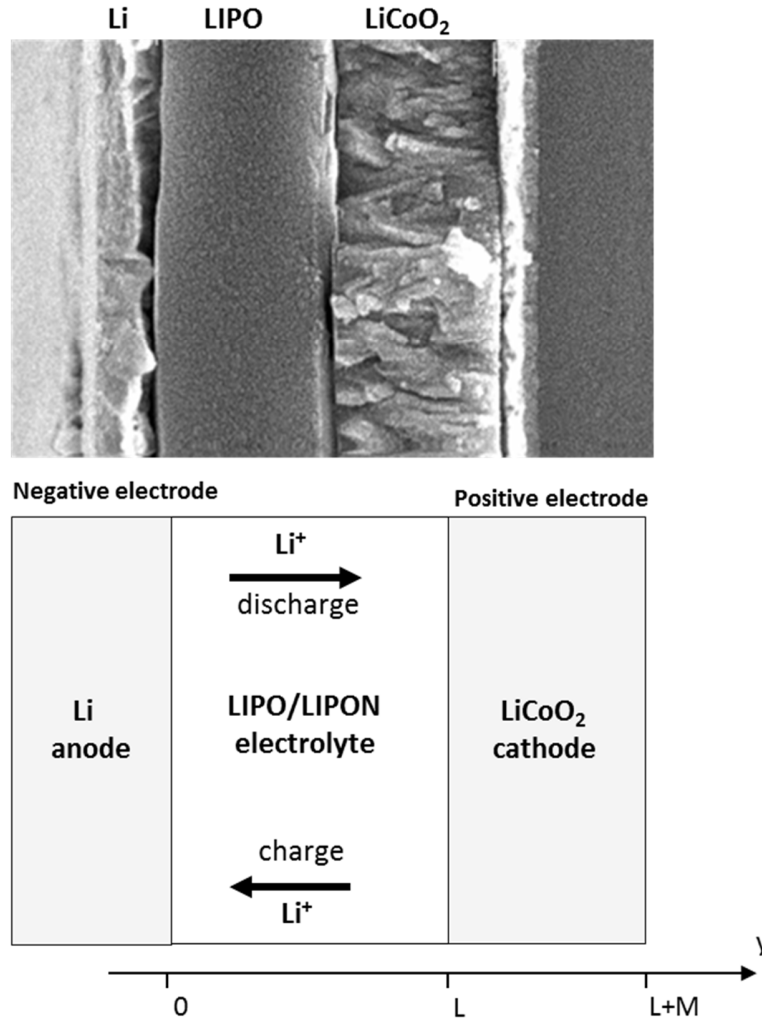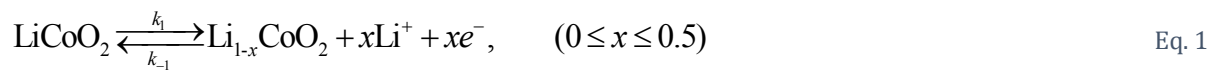

Fig. 1. Scanning Electron Microscopy image of a Li/LIPO/LiCoO₂ solid state battery and schematic layout for modeling planar all-solid-state cell.

$$\text{LiCoO}_2 \underset{k_{-1}}{\overset{k_1}{\rightleftharpoons}} \text{Li}_{1\text{-}x}\text{CoO}_2 + x\text{Li}^+ + xe^-, \qquad (0 \le x \le 0.5)$$

Eq. 1

$$\text{Li} \underset{k_{-2}}{\overset{k_2}{\rightleftharpoons}} \text{Li}^+ + e^- .$$

Eq. 2

The electrochemical kinetics of the charge transfer reactions, Eqs. 1 and 2, is modeled according to the Butler-Volmer equation. The Butler-Volmer equations for the positive and negative electrodes are represented by

$$I_{\mathrm{LiCoO_2}} = I^0_{\mathrm{LiCoO_2}} \left[e^{\alpha_{\mathrm{LiCoO_2}}\frac{F}{RT}\eta^{ct}_{\mathrm{LiCoO_2}}} - e^{-(1-\alpha_{\mathrm{LiCoO_2}})\frac{F}{RT}\eta^{ct}_{\mathrm{LiCoO_2}}} \right],$$ Eq. 3

$$I_{\mathrm{Li}} = I^0_{\mathrm{Li}} \left[e^{\alpha_{\mathrm{Li}}\frac{F}{RT}\eta^{ct}_{\mathrm{Li}}} - e^{-(1-\alpha_{\mathrm{Li}})\frac{F}{RT}\eta^{ct}_{\mathrm{Li}}} \right],$$ Eq. 4

respectively, where I_i and I^0_i ($i = \mathrm{LiCoO_2}, \mathrm{Li}$) represents the charge transfer reaction current and exchange current of lithium ions for each electrode [A], α_i is the charge transfer coefficient, F the Faraday constant (96485 C mol^{-1}), R the gas constant (8.314 J mol^{-1} K^{-1}), T the absolute temperature [K] and η^{ct}_i is the charge transfer overpotential [V]. The exchange currents for the positive and negative electrodes are accordingly defined as

$$I^0_{\mathrm{LiCoO_2}} = FAk^s_1 (\overline{c}_{\mathrm{CoO_2}}\overline{c}_{\mathrm{Li^+}})^{\alpha_{\mathrm{LiCoO_2}}} (\overline{c}_{\mathrm{LiCoO_2}})^{1-\alpha_{\mathrm{LiCoO_2}}}$$ Eq. 5

$$I^0_{\mathrm{Li}} = FAk^s_2 (\overline{c}_{\mathrm{Li^+}})^{\alpha_{\mathrm{Li}}} (\overline{c}_{\mathrm{Li}})^{(1-\alpha_{\mathrm{Li}})}$$ Eq. 6

where $k^s_1 = (k^0_1)^{(1-\alpha_{\mathrm{LiCoO_2}})}(k^0_{-1})^{\alpha_{\mathrm{LiCoO_2}}}$ and $k^s_2 = (k^0_2)^{(1-\alpha_{\mathrm{Li}})}(k^0_{-2})^{\alpha_{\mathrm{Li}}}$ are the standard rate constants for the charge transfer reaction in the positive and negative electrodes, A is the electrode surface area [m^2], and $\overline{c}_i$ [mol m^{-3}] is the bulk concentration of each reacting specie. When $\mathrm{Li^+}$ ions move from one electrode to another they must cross electrolyte layer. The ionic conductivity of the LIPO(N)-based solid-state electrolyte is caused by transport of $\mathrm{Li^+}$ ions only. According to the presented solid-state electrolyte model [7] Li in LIPO(N) matrix may reside in two types of states and assumes that the ionic conduction process is dominated by the ions, thermally occupying the higher energy (mobile) sites. The ionization reaction is given by

$$\mathrm{Li^0} \underset{k_r}{\overset{k_d}{\rightleftharpoons}} \mathrm{Li^+} + \mathrm{n^-},$$ Eq. 7

which describes the transfer process of immobile, oxygen-bonded lithium (indicated by Li^0) to mobile Li^+ ions. This reaction leaves behind uncompensated negative charges (n^-), which are associated to the nearest non-bridging oxygen atoms (nBO). In Eq. 7 parameter k_d is the rate constant for the ionic generation reaction [s^{-1}] and k_r is the rate constant for the recombination reaction [m^3 mol^{-1} s^{-1}]. Denote c_{Li^+} the concentration of mobile Li$^+$ ions [mol m^{-3}], c_{Li^0} the concentration of immobile Li ions [mol m^{-3}], c_{n^-} the concentration of n^- [mol m^{-3}] and c_0 the total concentration of Li atoms in the LIPO/LIPON matrix by [mol m^{-3}]. The fraction of Li, which resides in the mobile state under the equilibrium condition is denoted by δ, thus the equilibrium concentration of the charge carriers can be represented by $c_{Li^+}^{eq} = c_{n^-}^{eq} = \delta c_0$. Consequently, the equilibrium concentration of immobile lithium is represented by $c_{Li^0}^{eq} = (1-\delta)c_0$. The net rate of Li^+ generation is given by $r = k_d c_{Li^0} - k_r c_{Li^+} c_{n^-}$.

The ionic transport in the electrolyte is assumed to be a one-dimensional process described by the Nernst-Planck equation

$$J_j = -D_j \frac{\partial c_j}{\partial y} + \frac{z_j F}{RT} D_j c_j E,$$

Eq. 8

where $J_j(y,t)$ is the flux of species j [mol m^{-2} s^{-1}] at distance y from the surface of the negative electrode at any moment in time t, D_j is the diffusion coefficient of j [m^2 s^{-1}], $\partial c_j / \partial y$ the concentration gradient [mol m^{-4}], E the electric field [V m^{-1}], z_j the valence (dimensionless) and c_j is the concentration of species j [mol m^{-3}]. The two terms on the right-hand side of Eq. 8 represent the diffusion and migration contributions to the ionic flux. Denoting $r = k_d c_{Li^0} - k_r c_{Li^+} c_{n^-}$ and applying the electroneutrality condition $c(y,t) = c_{n^-}(y,t) = c_{Li^+}(y,t)$ it can be shown that the evolution of concentration $c(y,t)$ follows the diffusion equation according to

$$\frac{\partial c}{\partial t} = \frac{2D_{Li^+}D_{n^-}}{D_{Li^+}+D_{n^-}}\frac{\partial^2 c}{\partial y^2}+r,$$

$$c(y,0) = \delta c_0,$$

$$\frac{\partial c(0,t)}{\partial y} = \frac{I(t)}{2FAD_{Li^+}},$$

$$\frac{\partial c(L,t)}{\partial y} = \frac{I(t)}{2FAD_{Li^+}},$$

Eq. 9

where $I(t)$ is the current flowing through the battery. The electric field E follows an analytical expression

$$E(y,t) = \frac{RT}{F}\frac{1}{c(y,t)}\left\{-\frac{I(t)}{2FAD_{Li^+}}+\frac{D_{Li^+}-D_{n^-}}{D_{Li^+}+D_{n^-}}\left[\frac{\partial c(y,t)}{\partial y}-\frac{I(t)}{2FAD_{Li^+}}\right]\right\}.$$

Eq. 10

The total mass-transfer overpotential ($\eta_{Li^+}^{mt}$) across the LIPO(N) electrolyte is then given by

$$\eta_{Li^+}^{mt}(t) = \frac{RT}{F}\ln\left(\frac{c(L,t)}{c(0,t)}\right)-\int_0^L E(y,t)\mathrm{d}y.$$

Eq. 11

Assuming complete screening of Li ions in the cobalt oxide electrode one can expect that the mass transport of Li-ions inside the positive electrode can be described by the standard diffusion equation

$$\frac{\partial c_{LiCoO_2}}{\partial t} = \frac{\partial}{\partial y}\left(D_{Li}(c_{LiCoO_2}(y,t))\frac{\partial c_{LiCoO_2}}{\partial y}\right),$$

$$c_{LiCoO_2}(y,0) = c_{LiCoO_2}^0,$$

$$D_{Li}(c_{LiCoO_2}(L,t))\frac{\partial c_{LiCoO_2}(L,t)}{\partial y} = \frac{I(t)}{FA},$$

$$D_{Li}(c_{LiCoO_2}(L+M,t))\frac{\partial c_{LiCoO_2}(L+M,t)}{\partial y} = 0.$$

Eq. 12

where $c_{\mathrm{LiCoO_2}}(y,t)$ is concentration of $\mathrm{LiCoO_2}$ [mol m^{-3}] in location y at any moment of time t, $c^0_{\mathrm{LiCoO_2}}$ is the concentration of $\mathrm{Li^+}$ [mol m^{-3}] in the positive electrode at $t=0$ (in equilibrium) and $D_{\mathrm{Li}} = D_{\mathrm{Li}}(c_{\mathrm{LiCoO_2}}(y,t))$ is the diffusion coefficient [m^2 s^{-1}] of Li in the electrode, which is assumed to be concentration-dependent and will be specified in the subsequent sections. Eq. 12 shows how the profile develops as a function of time. Note that the normalised concentration of Li in the electrode can be defined as $x = c_{\mathrm{LiCoO_2}} / c^{\max}_{\mathrm{LiCoO_2}}$, where $c^{\max}_{\mathrm{LiCoO_2}}$ is the maximal concentration of Li in $\mathrm{LiCoO_2}$. Then the diffusion overpotential is calculated as

$$\eta^d_{\mathrm{LiCoO_2}} = E^{eq}_{\mathrm{LiCoO_2}}(x^s) - E^{eq}_{\mathrm{LiCoO_2}}(\overline{x}), \qquad\qquad\qquad \text{Eq. 13}$$

where $x^s = x(L,t)$ is the normalised surface concentration and $\overline{x}$ is the average bulk concentration. Finally, the total battery voltage is given by the summation of the equilibrium voltage and all overpotentials according to

$$E^{eq}_{bat} = E^{eq}_{\mathrm{LiCoO_2}} + \eta^d_{\mathrm{LiCoO_2}} + \eta^{ct}_{\mathrm{LiCoO_2}} + \eta^{ct}_{\mathrm{Li}} + \eta^{mt}_{\mathrm{Li^+}}. \qquad\qquad \text{Eq. 14}$$

Eq. 14 takes into account three main processes occurring inside the battery: diffusion in the $\mathrm{LiCoO_2}$ intercalation electrode, the charge transfer reaction at the surface of $\mathrm{LiCoO_2}$ and metallic Li electrodes, as given by Eqs. 3 and 4 accordingly, and the ionic flow through the solid-state electrolyte.

As it follows from the definition of the battery overvoltage during the discharge process, especially at the end, the diffusion of lithium in the cathode is the main limiting factor, affecting the voltage discharge curves. According to Eq. 12 the diffusion mass-transport mechanism is controlled by the diffusion coefficient D_{Li}. The diffusion coefficient can be described as the magnitude of the molar flux through a surface per unit concentration gradient [m^2 s^{-1}]. There is extensive experimental evidence that the diffusion coefficient in solid-state batteries is changing with the local State-of-Charge (SoC), see [12-17]. The reported values for diffusion coefficient of lithium in $\mathrm{LiCoO_2}$ are different for different composition

ranges. Table 1 includes the reported values from different studies on several $LiCoO_2$ cells. The bottom row of the table contains the difference between the expected values for the cathode materials with 003 plane direction, when the lithium ion diffusion pathways are parallel to the electrode-electrolyte interface plane, and cathode materials with 101 direction, when the Li-diffusion pathways are oriented perpendicular to the electrode-electrolyte interface. The Li-diffusion plane direction dependence for lithium cobalt oxide deposition plays therefore an important role in the quality of the fabricated cathode. Fig. 2a illustrates the experimentally measured diffusion coefficient as a function of SoC for references [12, 13, 19]. Table 1 and Fig. 2a clearly indicate that the diffusion coefficient behaves differently in three SoC regions, namely for $0.5 \le x < 0.8$, $0.8 \le x < 0.95$ and $x > 0.95$. According to the literature the reason for such behavior is phase-transition process in the cobalt oxide electrode. Region $x > 0.95$ corresponds to a single, solid-solution, lithium-rich phase, called phase I. Part $0.5 \le x < 0.8$ distinguishes a solid-solution region for phase II, which is less rich in lithium, while range $0.8 \le x < 0.95$ determines the two-phase coexistence area. Observing from Fig. 2a, that in the solid-solution regions diffusion coefficient still is SoC-dependent one can formulate a simple dependence of the $D_{Li}(x)$ on x as given in Fig. 2b, *i.e.* as piecewise linear function which remains continuous, but change the slope at the boundaries of the two-phase coexistence region at $x = 0.8$ and $x = 0.95$. Such a function approximates the experimentally observed $D_{Li}(x)$ by linear expressions of x and therefore c_{LiCoO_2}, while it assumes that in the two-phase coexistence region the diffusion coefficient is a weighted sum of the single-phase diffusion coefficients with the weights proportional to the amount of particular phase at given x. This formulation of $D_{Li}(x)$ was used to simulate the voltage discharge curves for the two datasets described in the previous section and for estimation of two sets of parameters corresponding to those datasets. Also note, that for the liquid electrolyte batteries concentration-dependent diffusion coefficients were used previously for modeling iron-phosphate batteries [21].

Resulting overall system of ordinary, partial and algebraic equations describing development of battery voltage as a function of applied current and time for given set of parameters was programmed in COMSOL Multiphysics 4.4.

Table I – Diffusivity of Li in $LiCoO_2$ measured with different techniques

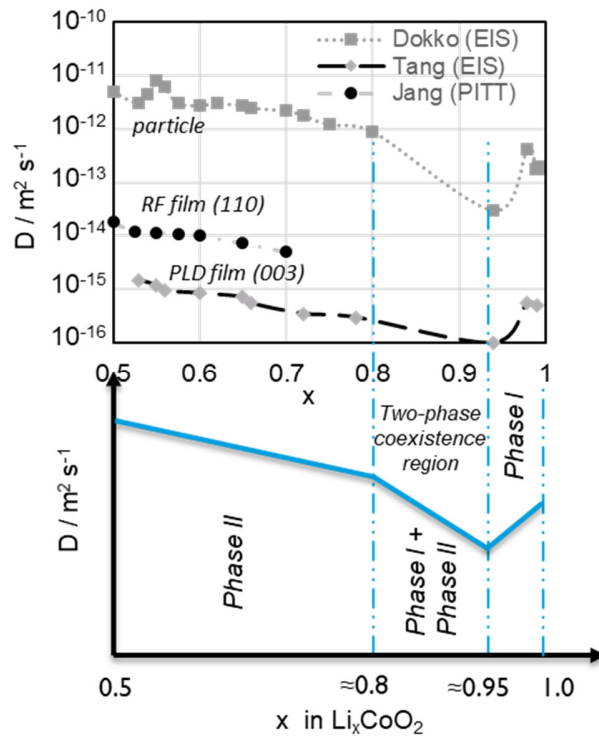| Material	Diffusivity [$m^2\ s^{-1}$]		Description	Ref.
$LiCoO_2$	10^{-14} to 10^{-12}			[12]
Li_xCoO_2	$4 \cdot 10^{-15}$ to $3 \cdot 10^{-13}$		$0.45 < x < 0.75$	[13]
Li_xCoO_2	$4 \cdot 10^{-15}$ to $3 \cdot 10^{-13}$ $1 \cdot 10^{-16}$		$0.45 < x < 0.75$ $x > 0.75$	[14] [15]
Li_xCoO_2	$1 \cdot 10^{-15}$ to $1 \cdot 10^{-13}$ $1 \cdot 10^{-16}$ No data reported		$0.45 < x < 0.75$ $0.75 < x < 0.95$ $x > 0.95$	[16] [16] [16]
Li_xCoO_2	(003)	(101)	Thin Film 003 Film (0.32 μm) 101 Film (1.60 μm)	[17] [17] [17]
	$1.6 \cdot 10^{-17}$ (PITT) $1.9 \cdot 10^{-17}$ (GITT) $1.6 \cdot 10^{-14}$ (EIS)	$1.8 \cdot 10^{-15}$ (PITT) $3.2 \cdot 10^{-15}$ (GITT) $6.0 \cdot 10^{-13}$ (EIS)		

Fig. 2. Estimation of diffusion coefficient for different LiCoO₂ cells by EIS measurements (a) and the suggested phase-transitions diagram (b).

Experimental

Experimental data used in this paper are represented by two datasets available in literature. The first one is a set of discharge curves from the original Danilov, *et al.* [7] paper, and further denoted as DNN. The discharge voltage curves were measured for Li/LIPO/LiCoO₂ thin-film solid state batteries with electrolyte thickness of 1.5 μm and a cathode thickness of 320 nm. Fig. 3a illustrates the equilibrium voltage (ElectroMotive Force, EMF) and 3 voltage discharge curves for this dataset. The second dataset represents discharge curves from paper [22], further denoted as NDB, where a Li/LIPON/LiCoO₂ cell was investigated with 3 μm of Li, 1 μm of LIPON and a cathode with thickness of 1.8 μm. Again, the equilibrium voltage curve and 3 voltage discharge curves with comparable C-rates are shown. Fig. 3b shows EMF and 3 discharge voltage curves for that dataset.
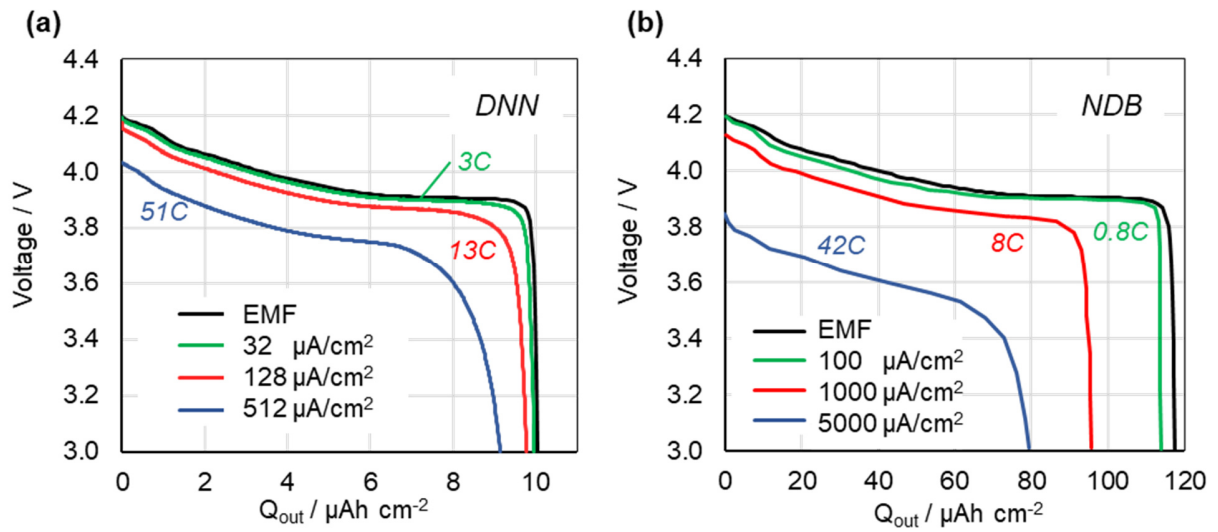
Fig. 3. EMF and experimental voltage discharge curves for DNN (a) and NDB (b) cells.

Results and Discussion

Illustration of the performance of the model with concentration dependent diffusion coefficient is given by Fig. 4. In particular, Fig. 4a deals with the DNN experiments, Fig. 4b corresponds to those of NDB. In Fig. 4a the experimental data are given by black dots, while green solid lines correspond to the model with concentration dependent diffusion coefficient estimated from the same DNN dataset (DNN column in Table II). In Fig. 4b the experimental data are shown again as black dots. The green solid lines correspond to model with all coefficients estimated from the same NDB dataset (NDB column in Table II), and the diffusion coefficient taken concentration-dependent. Values for the concentration dependent diffusion coefficient and constant diffusion coefficient are the result of optimization on rough grid. For all models, one can see an almost perfect agreement between the experimental data and simulations with estimated parameters at low C-rates. However, this agreement declines towards very high discharge currents as Fig. 4b reveals.
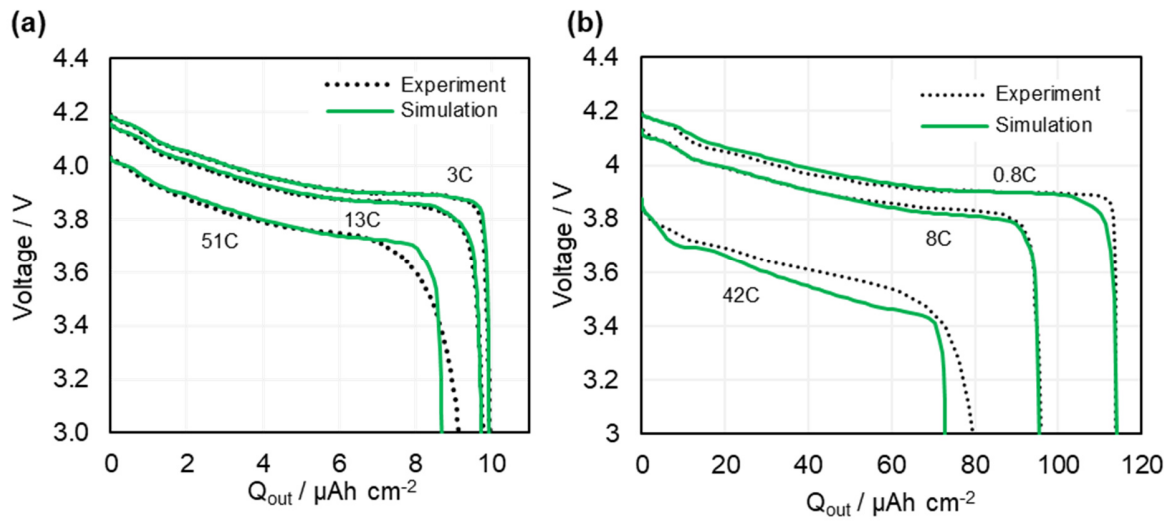
Fig. 4. (a) Discharge voltage vs capacity profiles for DNN experiment, experimental data – black dots, simulation model – solid green lines, (b) Discharge voltage vs capacity profiles for NDB experiment, experimental data – black dots, simulation model with diffusion coefficient taken from DNN fit – blue lines, simulation model with fitted diffusion coefficient – solid green lines.

Fig. 5a illustrates the choice of concentration dependent diffusion coefficients. The black dots and curves in Fig. 5a denotes the same experimental data as shown in Fig. 2, *i.e.* taken from [12, 13, 19]. The blue line illustrates average constant diffusion coefficient of $1.3 \cdot 10^{-14}\,m^2\,s^{-1}$. The corresponding discharge curves are shown in Fig. 5b by blue lines. Strong deviation from experimental results is apparent. The red line in Fig. 5a shows the variable diffusion coefficient as function of degree of lithiation x in the positive electrode as it comes out of estimation on DNN dataset. The corresponding discharge curves are shown by the red lines in Fig. 5b. One can see that deviation from the experimental data reduces, but still remains strong. Apparently, the same parameters for diffusion coefficient cannot be used simultaneously for both datasets. The green line in Fig. 5a corresponds to the vertical shift of whole profile towards higher values in logarithmic scale, corresponding discharge curves are plotted as green lines in Fig. 5b. That formulation provides best agreement with experimental data.

Table II. Sets of parameters used in simulations

Parameter	Unit	DNN		NDB	
c_0	mol m^{-3}	60100		62000	
δ	-	0.04		0.04	
k_d	s^{-1}	$9.0 \cdot 10^{-7}$		$9.0 \cdot 10^{-7}$	
k_r	m^3 mol^{-1} s^{-1}	$9.0 \cdot 10^{-9}$		$9.0 \cdot 10^{-9}$	
D_{Li^+}	m s^{-2}	$6.0 \cdot 10^{-15}$		$22.0 \cdot 10^{-15}$	
D_{n^-}	m s^{-2}	$6.0 \cdot 10^{-17}$		$22.0 \cdot 10^{-17}$	
$c_{LiCoO_2}^{max}$	mol m^{-3}	23300		48760	
$c_{LiCoO_2}^{0}$	mol m^{-3}	11650		24380	
α_{LiCoO_2}	-	0.6		0.6	
α_{Li}	-	0.5		0.5	
D_{Li}	m s^{-2}	x=0.50	$8.5 \cdot 10^{-14}$	x=0.50	$2.0 \cdot 10^{-13}$
		x=0.80	$2.5 \cdot 10^{-14}$	x=0.80	$6.0 \cdot 10^{-14}$
		x=0.95	$5.0 \cdot 10^{-16}$	x=0.95	$2.0 \cdot 10^{-15}$
		x=1.00	$7.0 \cdot 10^{-15}$	x=1.00	$1.4 \cdot 10^{-14}$

A number of parameter values, such as k_d, k_r α_{Li}, α_{LiCoO_2} and δ are the same for both set of simulations, some other have only minor differences, for example c_0. In other cases differences are larger. In particular, 3.5 times larger values of D_{Li^+} and D_{n^-} for the case of NDB can be explained by better performance of LIPON in comparison with LIPO. Difference in values of D_{Li} are related to the different deposition process of the LCO material used for NDB cells, which increased Li-ion diffusion. This is further supported by the increased capacity and density of the material which appear from changes in $c_{LiCoO_2}^{max}$ and $c_{LiCoO_2}^{0}$, *i.e.* a higher packing density and electro-activity obtained for NDB cells is favourable for Li-ion diffusion.
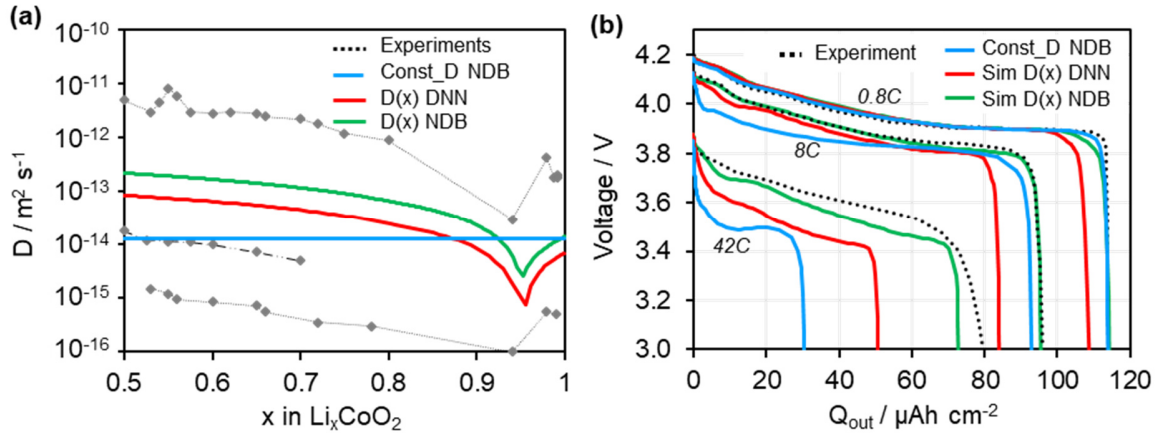

Fig. 5. (a) Behavior of diffusion coefficient for DNN set of parameters (red line) in comparison with available experimental measurements (grey lines and dots) and suggested modification of diffusion coefficient formulation to apply in NDB dataset modeling (green line). Blue line represents average constant diffusion coefficient. (b) NDB improvements in predicting discharge curves: experimental (dotted lines), simulated with diffusion coefficient taken from DNN (red lines) and the best fit (green lines) which corresponds to the diffusion coefficient formulation shown in Fig. 5a (green line). Simulations with constant diffusion coefficient are shown by blue lines.

The electrochemical performance of the model for both datasets is shown in Fig. 6, where (a) relates to DNN set of parameters while (b) reproduces similar plots for NDB. In both figures the bottom plot illustrates the development of $c(y,t)$ and $c_{LiCoO_2}(y,t)$ in the electrolyte and cobalt oxide electrode, accordingly, while the top inset contains behaviour of D_{Li} across the cobalt oxide electrode. Three

coloured lines in the plots corresponds to the beginning (red), the middle (blue) and the end (red) of 51 C-rate discharging. $c(y,t)$ profiles for both datasets show deviations from the average value only near
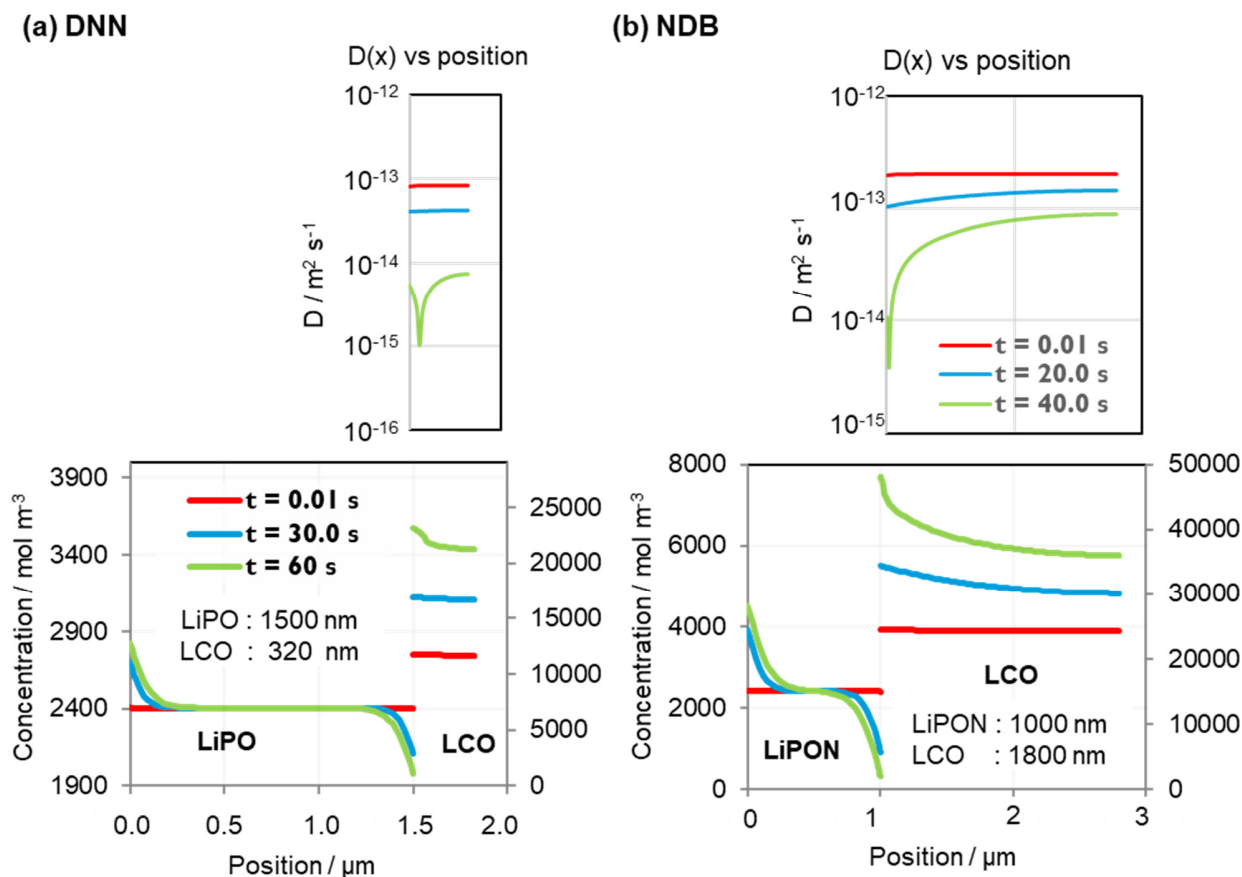

Fig. 6. (a) Behavior of lithium concentration profiles across the thin-film battery for DNN set of parameters (bottom plot) and diffusion coefficient in cobalt oxide electrode as function of position (top inset). Three colored lines refer to three subsequent moments of time, corresponding to begin of discharging (red line), middle and end of discharging (blue and green lines accordingly), 51C rate is applied. (b) The same electrochemical plots reproduced according to NDB set of parameters are comparable C-rate.

the boundaries with electrodes. In contrast, $c_{\text{LiCoO}_2}(y,t)$ in both plots systematically growth, indicating lithiation of cobalt oxide electrode during discharging. It is interesting to observe that for DNN set of parameters the high rate discharge caused non-monotonous behaviour of diffusion coefficient across the electrode, which also creates 'kink' in $c_{\text{LiCoO}_2}(y,t)$ concentration profile in corresponding place, see Fig. 6a. NDB set of parameters have higher values of diffusion coefficients implying practically monotonous

behaviour of diffusion coefficient, see top plot in Fig. 6b. In addition, the concentration profiles in Figs. 6 nicely illustrate that the diffusion coefficient of the cathode material is a main factor limiting rate performance when going to thicker films (*e.g.* 3 μm) and/or higher C-rates. As can be seen from Fig. 4, the extracted capacity drops much more for the NDB cathode with 3 μm thickness (even with a higher diffusion constant as appears from the simulation fitting) which is concerted with a much steeper concentration gradient at end-of-discharge as shown in Fig. 6. Limited by the cathode diffusion constant, the concentration in the bulk of the cathode develops more slowly for the thicker film resulting in lower overall capacity at end-of-discharge, *i.e.* when overpotentials increase sharply as the maximum concentration is reached at the interface. These observations are relevant for ultrafast charging application where >5 C is desired: the improved model enables a method to optimize thickness of the cathode end electrolyte for both rate performance and high energy density TFSSB.

Conclusions

A simulation approach for TFSSB had been developed which overcomes the drawback of available mathematical models, *i.e.* the inaccuracy of existing models at high currents. The simulation results and parameter estimations were presented for one-dimensional electrochemical model, which includes the charge transfer kinetics at the electrolyte-electrode interface, diffusion and migration in the electrolyte as well as diffusion of Li-ions in the intercalation electrode. The diffusion coefficient in the $LiCoO_2$ cathode is a function of local lithiation degree and takes into account phase-transition processes. It was shown that the model and estimation procedure work well for two available datasets, providing good agreement with the experiments even up to very high C-rates. Therefore, introducing the functional dependence of the diffusion coefficient on the lithium concentration have shown to be a valuable improvement of the mathematical models for Li-ion TFSSB.

Acknowledgement

References

[1] J. M. Tarascon, M. Armand, Nature (2001), 414, 359.

[2] V. Ramadesigan, P. W. C. Northrop, S. De, S. Santhanagopalan, R. D. Braatz, and V. R. Subramanian, Journal of the Electrochemical Society (2012), 159, R31.

[3] Manthiram, Lithium Batteries: Science and Technology (Eds: G. A. Nazri, G. Pistoia), Springer, New York 2009, Ch. 1.

[4] Lithium-Ion Battery Market Shares, Strategies, and Forecasts, Worldwide, 2011 to 2017, Market Research Store, Code: MRS - 2397.

[5] R. Spotnitz, J. Franklin, Journal of Power Sources (2003), 113 (1), 81-100.

[6] K. Takada, Acta Materialia (2013), 61 (3), 759-770.

[7] D. Danilov, R. A. H. Niessen, P. H. L. Notten, Journal of the Electrochemical Society (2011), 158, A215-A222.

[8] S. D. Fabre, D. Guy-Bouyssou, P. Bouillon, F. Le Cras, C. Delacourt, Journal of the Electrochemical Society (2012), 159, A104-A115.

[9] M. Jagannathan, K.S.R. Chandran, K.S. Ravi, Journal of Power Sources (2014), 247, 667-675.

[10] R. Chandrasekaran, Journal of Power Sources (2014), 262, 501-513.

[11] R. Behrou, K. Maute, Journal of the Electrochemical Society (2017), 164 (12), A2573-A2589.

[12] K. Dokko, M. Mohamedi, Y. Fujita, T. Itoh, M. Nishizawa, M. Umeda, I. Uchida, Journal of the Electrochemical Society (2001), 148 (5), A422–A426.

[13] Y. Jang, B. J. Neudecker, N. J. Dudney, Electrochemical and Solid-State Letters (2001), 4 (6), A74–A77.

[14] J. Barker, R. Pynenburg, R. Koksbang, M.Y. Saidi, Electrochimica Acta (1996), 41 (15), 2481–2488.

[15] M. Okubo, E. Hosono, T. Kudo, H. S. Zhou, I. Honma, Solid State Ionics (2009), 180, 612–615.

[16] N. J. Dudney, Y. Jang, Journal of Power Sources (2003), 119-121, 300–304.

[17] J. Xie, N. Imanishi, T. Matsumura, O. Yamamoto, Solid State Ionics (2008), 179(9), 362–370.

[18] A. Van der Ven, G. Ceder, Electrochemical and Solid-State Letters (2000), 3 (7), 301–304.

[19] S. B. Tang, M. O. Lai, L. Lu, Journal of Alloys and Compounds (2008), 449, 300-303.

[20] P. J. Bouwman, B. A. Boukamp, H. J. M. Bouwmeester, P. H. L. Notten, Journal of the Electrochemical Society (2002), 149, A699.

[21] M. Farkhondeh, C. Delacourt, Journal of the Electrochemical Society (2012), 159 (2), A177-A192.

[22] B. J. Neudecker, N. J. Dudney, J. B. Bates, Journal of the Electrochemical Society (2000), 147 (2), 517-523.